Geophysical Research Letters

RESEARCH LETTER
10.1029/2020GL091327

Venus' Mass Spectra Show Signs of Disequilibria in the Middle Clouds

Rakesh Mogul[1,2], **Sanjay S. Limaye**[3], **M. J. Way**[4,5,6], **and Jaime A. Cordova**[7]

[1]Chemistry & Biochemistry Department, California State Polytechnic University, Pomona, Pomona, CA, USA, [2]Blue Marble Space Institute of Science, Seattle, WA, USA, [3]GSFC Sellers Exoplanet Environments Collaboration, Greenbelt, MD, USA, [4]Department of Physics and Astronomy, Theoretical Astrophysics, Uppsala University, Uppsala, Sweden, [5]Laboratory of Genetics, University of Wisconsin, Madison, WI, USA, [6]NASA Goddard Institute for Space Studies, New York, NY, USA, [7]Space Science and Engineering Center, University of Wisconsin, Madison, WI, USA

Key Points:

- Mass data from the Pioneer Venus Large Probe Neutral Mass Spectrometer reveals several trace chemical species suggestive of disequilibria
- Trace species in the middle clouds include phosphine, hydrogen sulfide, nitrous acid, nitric acid, hydrogen cyanide, and carbon monoxide
- Data reveal chemicals related to anaerobic phosphorus metabolism (phosphine), anoxygenic photosynthesis (nitrite), and the nitrogen cycle

Supporting Information:

Supporting Information may be found in the online version of this article.

Correspondence to:

R. Mogul,
rmogul@cpp.edu

Citation:

Mogul, R., Limaye, S. S., Way, M. J., & Cordova, J. A. (2021). Venus' mass spectra show signs of disequilibria in the middle clouds. *Geophysical Research Letters*, *48*, e2020GL091327. https://doi.org/10.1029/2020GL091327

Received 21 OCT 2020
Accepted 2 MAR 2021

Author Contributions:

Conceptualization: Rakesh Mogul
Data curation: Rakesh Mogul, M. J. Way
Formal analysis: Rakesh Mogul, Sanjay S. Limaye, M. J. Way, Jaime A. Cordova
Methodology: Rakesh Mogul
Visualization: Rakesh Mogul
Writing – original draft: Rakesh Mogul
Writing – review & editing: Rakesh Mogul, Sanjay S. Limaye, M. J. Way, Jaime A. Cordova

Abstract We present a re-examination of mass spectral data obtained from the Pioneer Venus Large Probe Neutral Mass Spectrometer. Our interpretations of differing trace chemical species are suggestive of redox disequilibria in Venus' middle clouds. Assignments to the data (at 51.3 km) include phosphine, hydrogen sulfide, nitrous acid, nitric acid, carbon monoxide, hydrochloric acid, hydrogen cyanide, ethane, and potentially ammonia, chlorous acid, and several tentative P_xO_y species. All parent ions were predicated upon assignment of corresponding fragmentation products, isotopologues, and atomic species. The data reveal parent ions at varying oxidation states, implying the presence of reducing power in the clouds, and illuminating the potential for chemistries yet to be discovered. When considering the hypothetical habitability of Venus' clouds, the assignments reveal a potential signature of anaerobic phosphorus metabolism (phosphine), an electron donor for anoxygenic photosynthesis (nitrite), and major constituents of the nitrogen cycle (nitrate, nitrite, ammonia, and N_2).

Plain Language Summary We re-examined archived data obtained by the Pioneer Venus Large Probe Neutral Mass Spectrometer (LNMS). Our results reveal the presence of several trace chemical species in Venus' clouds including phosphine, hydrogen sulfide, nitrous acid (nitrite), nitric acid (nitrate), hydrogen cyanide, and possibly ammonia. The presence of these chemicals suggest that Venus' clouds are not at equilibrium; thereby, illuminating the potential for chemistries yet to be discovered. Furthermore, when considering the potential habitability of Venus' clouds, our work reveals a potential signature of anaerobic phosphorus metabolism (phosphine), along with key chemical contributors toward anoxygenic photosynthesis (nitrite) and the terrestrial nitrogen cycle (nitrate, nitrite, possibly ammonia, and N_2).

1. Introduction

Venus' clouds harbor several proposed trace chemical species that suggest the potential for chemistries yet to be discovered. Exemplar trace species include ammonia, oxygen, hydrogen, methane, and ethene, which were detected remotely or in situ (Kumar et al., 1981; Moroz, 1981; Oyama et al., 1980; Pollack et al., 1993; Smirnova & Kuz'min, 1974; Surkov, 1977). Recently, phosphine was reported by Greaves, Richards, Bains, Rimmer, Sagawa, et al. (2020), with both the detection and interpretation as a biosignature spurring significant debate within the community (Bains et al., 2020; Encrenaz et al., 2020; Greaves, Bains, et al., 2020; Greaves, Richards, Bains, Rimmer, Clements, et al., 2020; Snellen et al., 2020; Villanueva et al., 2020). In this context, we sought to examine available in situ data for signatures of trace species at Venus. Given the recent interest in the potential habitability of the lower/middle cloud deck (Greaves, Richards, Bains, Rimmer, Sagawa, et al., 2020; Limaye et al., 2018; Seager et al., 2020), we concentrated on data obtained from within the clouds by the Pioneer Venus (PV) Large Probe Neutral Mass Spectrometer (LNMS), which sampled the atmosphere during descent on December 9, 1978 (Hoffman, Hodges, & Duerksen, 1979).

To date, the LNMS-related literature predominantly discusses atmospheric components, such as CO_2, N_2, and the noble gases, with little attention given to trace/minor species, apart from methane and water (Donahue et al., 1982; Donahue and Hodges, 1992, 1993; Hoffman, Hodges, Donahue, et al., 1980; Hoffman, Hodges, Wright, et al., 1980; Hoffman, Hodges, & Duerksen, 1979; Hoffman, Oyama, et al., 1980; Hoffman et al., 1979a, 1979b). The LNMS data were additionally discussed by Von Zahn and Moroz (1985), as part

of the Venus International Reference Atmosphere Model (Kliore et al., 1985). A comprehensive but not exhaustive list from Venus observations (space and ground) can be found in Johnson and de Oliveira (2019). Beyond these studies, there is limited information on the assignment of trace chemicals, and fragmentation products, in the LNMS data.

In this study, we present a re-assessment of the LNMS mass spectral data obtained in the middle clouds (Figure 1a). The data in focus from an altitude of 51.3 km was originally published in identical tables in Hoffman, Hodges, Donahue, et al. (1980) and Hoffman, Hodges, Wright, et al. (1980). In total, our interpretations match and expand upon the original LNMS studies (Hoffman et al., 1979b; Hoffman, Hodges, Donahue, et al., 1980), with these new analyses revealing the potential presence of reduced chemicals in the middle clouds, including phosphine (PH_3), hydrogen sulfide (H_2S), nitrous acid (HNO_2), carbon monoxide (CO), ethane (C_2H_6), and potentially ammonia (NH_3), and chlorous acid ($HClO_2$). This composition is accordingly suggestive of redox disequilibria within Venus' clouds.

1.1. Data and Methods

The LNMS contained a magnetic sector-field mass analyzer (Hoffman, Hodges, Donahue, et al., 1980), and sampled gases through a pair of metal inlet tubes (3.2 mm diameter), which were pinched at the ends that extended into the atmosphere. Data were collected from 64.2 km toward the surface, where 38 spectra were recorded at the ionization energy of 70 eV (barring the incomplete spectrum at the surface). Between ~50 and 25 km, the LNMS experienced a clog due to aerosol solutes, indicated as sulfuric acid by Hoffman, Hodges, Donahue, et al. (1980), which ultimately cleared at the higher temperatures at lower altitudes. The main focus of this report was spectra obtained from 64.1 to 51.3 km before the clog.

During the descent, ion counts were obtained at 232 pre-selected mass positions between 1 and 208 amu and integrated over 235 ms by an on-board microprocessor. Per Hoffman, Hodges, and Duerksen (1979), in-flight corrections between measurements were performed using calibrants at 15 (CH_3^+), 68 ($^{136}Xe^{++}$), and 136 ($^{136}Xe^+$) amu to control the ion acceleration voltage and adjust for the impacts of temperature and other factors during descent. Information regarding corrections to the pre-selected amu values were not included in the archive data, nor were example *m/z* profile data, statistical insights into the measurements, or control spectra. For this study, therefore, peak shapes and shifts to the measured amu values were estimated using the LNMS count data, which contained sufficient mass points to approximate the profiles for CH_3^+ (15 amu), H_2O^+ (18 amu), CO^+ (28 amu), N_2^+ (28 amu), $^{40}Ar^+$ (40 amu), and $^{136}Xe^+$ (136 amu)— which were presumed to be pre-selected species since the respective exact masses (Haynes, 2016; Roth et al., 1976) were identical or very close to the pre-selected mass values (see supporting information).

Mass profiles from 51.3 km for these six pre-selected species, or references (inclusive of the CH_3^+ and $^{136}Xe^+$ calibrants) are displayed in Figures 1b–1f, while those between 64.2 and 55.4 km are provided in Figure S1. Reasonable fits were obtained using the Gauss function (Stark et al., 2015; Urban et al., 2014), where regressions were unconstrained and minimized by least squares for profiles possessing >3 points per peak, and by least absolute deviations (LADs) for those with ≤3 points per peak. Regression outputs provided peak heights (calculated counts), peak means (calculated mass or amu at the centroids), and standard deviations. In turn, these terms were converted to the estimated full width half maximum (FWHM) and the difference between the calculated and expected mass (Δamu) for each respective species.

As shown in Figure 1g, calculated masses obtained across the altitudes of 64.2– 51.3 km were 15.022 ± 0.001, 18.003 ± 0.001, 27.996 ± 0.001, 28.006 ± 0.003, 39.967 ± 0.004, and 135.926 ± 0.012 amu—which was indicative of the pre-selected values shifting with altitude and increasing with increasing amu. Across 64.2–51.3 km, the total shifts (Δamu, absolute) ranged from 0.000 to 0.013 amu between 15 and 40 amu, and increased up to 0.030 amu at 136 amu. Across 55.4–51.3 km, the range was smaller at 0.000–0.009 amu across 15–136 amu. For measurements in the middle clouds (55.4–51.3 km), this was suggestive of minimal changes to the pre-selected mass positions.

Per Figure 1h, plotting of FWHM for the six references against the calculated amu revealed a linear relationship ($R^2 = 0.994$). Hence, we leveraged this trend to estimate the FWHM of poorly sampled mass peaks. For target species, the estimated FWHM and standard deviation were obtained using the linear trend at the respective altitude. In turn, regressions to poorly sampled mass peaks (<40 amu) were minimized using

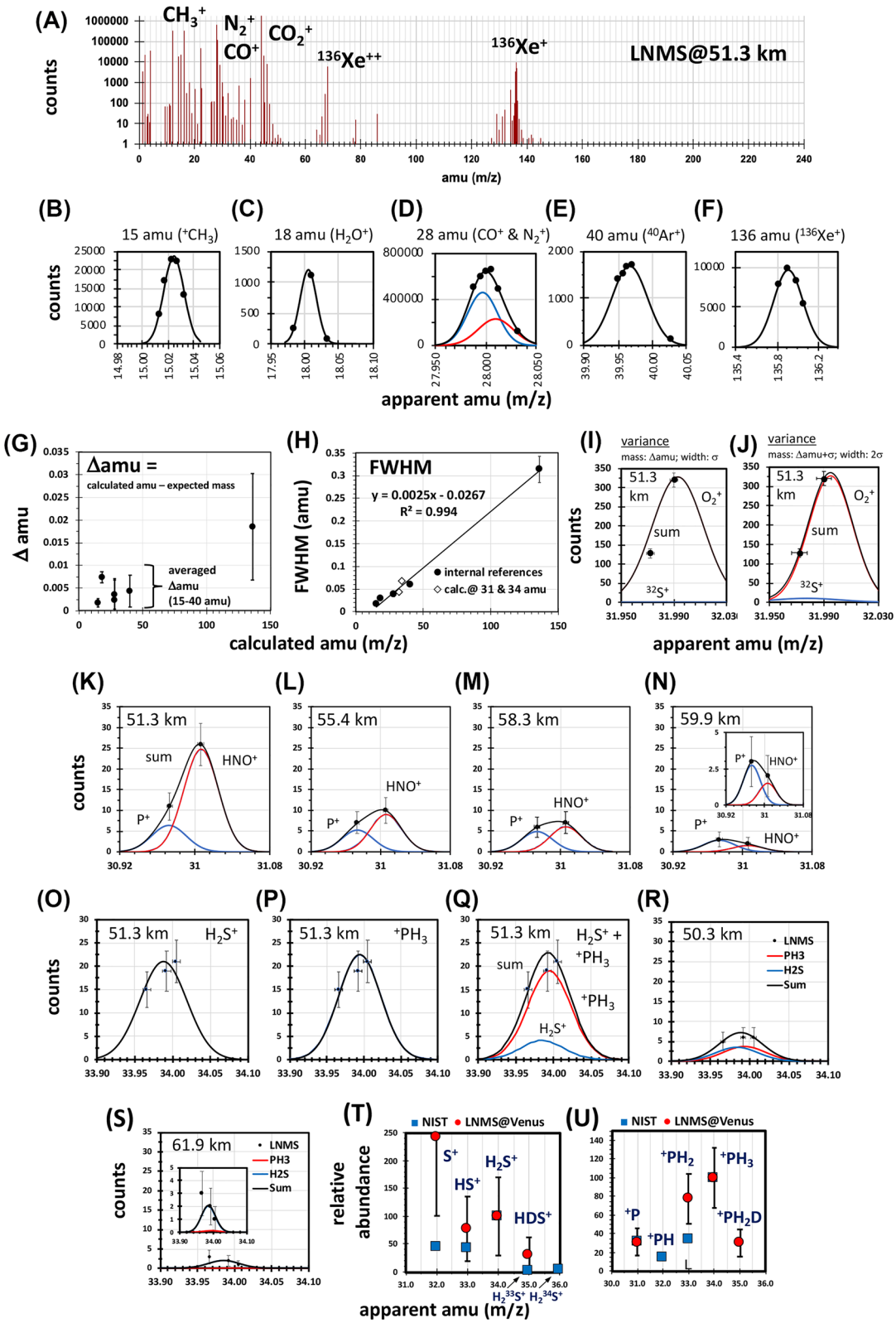
(A)
counts
amu (m/z)
LNMS@51.3 km
(B) 15 amu (+CH3)
(C) 18 amu (H2O+)
(D) 28 amu (CO+ & N2+)
(E) 40 amu (40Ar+)
(F) 136 amu (136Xe+)
apparent amu (m/z)
(G) Δamu = calculated amu – expected mass
averaged Δamu (15-40 amu)
(H) FWHM
y = 0.0025x - 0.0267
R² = 0.994
internal references
calc.@ 31 & 34 amu
calculated amu (m/z)
(I) variance
mass: Δamu; width: σ
(J) variance
mass: Δamu+σ; width: 2σ
apparent amu (m/z)
(K) 51.3 km
(L) 55.4 km
(M) 58.3 km
(N) 59.9 km
(O) 51.3 km
(P) 51.3 km
(Q) 51.3 km
(R) 50.3 km
LNMS
PH3
H2S
Sum
(S) 61.9 km
(T) NIST LNMS@Venus
relative abundance
apparent amu (m/z)
(U) NIST LNMS@Venus

LAD, and constrained using the estimated FWHM (using the standard deviation as the variance) and target expected mass (using a variance that equaled the averaged Δamu obtained between 15 and 40 amu at the respective altitude). Calculated FWHM values obtained from LAD minimizations for 31 to 34 amu (at 51.3 km) are plotted as diamonds in Figure 1h and retain the trend of the references. Additionally, fits at 16 amu for O^+ and $CH_4{}^+$ (Figure S2) provided a resolving power between the mass pairs of 471 (valley minima at 12% of the O peak), which was functionally similar to the reported LNMS value of ≥440 (valley minima at 9% of O) (Hoffman, Hodges, Wright, et al., 1980).

Accordingly, we re-assessed the LNMS data to identify trace and minor species. In this model, chemical identities were predicated upon the assignment of atomic species, fragmentation products, and isotopologues (if so possible) to parent ions, and vice versa, where parent ions with no associated fragments, and fragments with no associated parent ions, were considered tentative. Among the many limitations to this approach, however, included a reliance upon Gauss fits and estimated FWHM, and an inability to account for potential ion scattering within the mass analyzer.

2. Results

2.1. Overview

Parent species assigned to the LNMS data are summarized in Table 1 and following sections, where the associated apparent amu is provided for reference (bold amu values represent the exact mass). Fragments and isotopologues of key parents are detailed in Table S1. Unique to this analysis was the identification of atomic phosphorous ($^+$P) in the data. Across the masses, isotopologues containing ^{2}H (D), ^{13}C, ^{15}N, ^{18}O, ^{33}S, ^{34}S, and ^{37}Cl were observed; as were the atomic ions of ^{20}Ne, ^{21}Ne, ^{22}Ne, ^{36}Ar, ^{38}Ar, and ^{40}Ar. The most abundant parent ion in the data was $CO_2{}^+$. Polyatomic ions included COS^+, $SO_2{}^+$, and $NO_2{}^+$, and diatomic ions included $N_2{}^+$, $O_2{}^+$, CO^+, NO^+, SO^+. Assigned acidic species (weak and strong) included water, fragments consistent with sulfuric acid, and the monoprotic acids of nitrous acid (HNO_2), nitric acid (HNO_3), hydrochloric acid (HCl), hydrogen cyanide (HCN), and possibly hydrofluoric acid (HF), and chlorous acid ($HClO_2$).

Fragmentation patterns for carbon dioxide (CO_2) from the LNMS data (Table S1) and NIST mass spectral reference are displayed in Figure S3. The presence of CO_2 was evident by observation of the parent ion ($CO_2{}^+$), double-charged parent ion ($CO_2{}^{++}$), all fragments (CO^+, O^+, and C^+), and the isotopologues of $^{13}CO_2$, $CO^{18}O$, ^{13}CO, and $C^{18}O$. Relative abundances for CO^+, O^+, and C^+ were higher in the LNMS, which was suggestive of enrichment from atmospheric CO. Counts across most altitudes (barring 50–25 km, due to the clog) were supportive of a $^{13}C/^{12}C$ isotope ratio of $1.33 \times 10^{-2} \pm 0.01 \times 10^{-2}$, and $^{18}O/^{16}O$ ratio of $2.18 \times 10^{-3} \pm 0.17 \times 10^{-3}$.

2.2. Hydrogen Sulfide and Phosphine

Table S1 lists the mass data (51.3 km) and assignments for hydrogen sulfide (H_2S) and phosphine (PH_3) along with the associated fragments and isotopologues. Due to similar masses for H_2S^+ and $^+PH_3$, as well as HS^+ and $^+PH_2$ (Δm values of 0.009661), resolving powers beyond the capabilities of the LNMS (3519 and 3414) would be required for separation. Therefore, unambiguous assignments for the parent ion (M^+) and

Figure 1. (a) LNMS spectra obtained at 51.3 km with annotations for the major species and in-flight calibrants. (b–f) Approximate peak shapes at 51.3 km obtained from regressions of the mass points at 15 amu ($CH_3{}^+$), 18 amu (H_2O^+), 28 amu (CO^+ & $N_2{}^+$), 40 amu ($^{40}Ar^+$), and 136 amu ($^{136}Xe^+$); *y*-axis error bars are smaller than marker size of the data points. (g and h) Relationships between calculated amu and Δamu (Δamu = calculated amu – expected mass) and full width half maximum (FWHM), where averages and standard deviations (error bars) were calculated across the altitudes between 64.2 and 51.3 km (most error bars are smaller than the marker size); diamonds represent the calculated FWHM from deconvolutions at 31 and 34 amu. (i and j) Fits to the mass pair at 32 amu at 51.3 km showing $^{32}S^+$ (blue), $O_2{}^+$ (red), and summed value (black) using differing variances for the mass and FWHM terms. (k–n) Fits to the mass pair at 31 amu for P^+ (blue), HNO^+ (red), and summed value (black) across 59.9–51.3 km; *x*-axis error bars represent the standard deviation for the averaged Δamu (between 15 and 40 amu) at the respective altitude, and *y*-axis error bars represent the square root of the counts. (o–q) Fits to the mass triplet at 34 amu from 51.3 km for PH_3 (red), H_2S (blue), and a composite of PH_3 and H_2S; plot layout and error bars are as described above. (r and s) Fits to the mass triplet at 34 amu from 50.3 and 55.4 km for a composite of PH_3 (red) and H_2S (blue); plot layout and error bars are as described. (t and u) Comparison of fragmentation patterns for PH_3 and H_2S from the LNMS data (red circles) and the respective NIST mass spectral references (blue squares); counts for S^+, H_2S^+, HDS^+, ^+P, $^+PH_3$, and $^+PH_2D$ were obtained as described, while counts for $^+PH_2$ and HS^+ were disambiguated using the relative abundances of the parent species; error bars represent the square root of the counts, and masses are displayed in unit resolution for clarity.

Table 1
Assignment of Parent Species in the LNMS Data at 51.3 km, Where LNMS amu Represents the Pre-Selected or Apparent amu Value

LNMS amu	Count[a]	Identity[b]	Expected mass	LNMS amu	Count[a]	Identity[b]	Expected mass
2.016	22,016	**H_2**	2.014102	31.990	327[d]	**O_2**	31.990000
16.031	39,936	**CH_4**	16.031300	33.992	19[d]	**PH_3**	33.997382
17.026	244	*NH_3*	17.026549		4[d]	**H_2S**	33.987721
		$^{13}CH_4$	17.034655	35.005	6[d]	**PH_2D**	35.003659
18.010	1,200[d]	**H_2O**	18.010650		1[d]	**HDS**	34.993998
18.034	20[d]	*NH_2D*	18.034374	35.981	3[d]	**HCl**	35.976678
20.006	112	*HF*	20.006228	43.991	1,769,472	**CO_2**	43.990000
20.015	30	**$H_2{}^{18}O$**	20.014810	44.991	21,504	**$^{13}CO_2$**	44.993355
		D_2O	20.023204	44.991	7,936	**$CO^{18}O$**	44.993355
27.010	77[d]	**HCN**	27.010899	47.000	94	**HNO_2**	47.000899
27.988	423,535[d]	**CO**	27.995000	59.966	1	*COS*	59.967071
28.012	278,529[d]	**N_2**	28.012130	62.994	1	**HNO_3**	62.995899
28.032	≤50[d]	**C_2H_4**[c]	28.031300	63.962	5	**SO_2**[c]	63.962071
28.997	7,040[d]	**^{13}CO**	28.998355	65.961	0.3[d]	**$^{34}SO_2$**[c]	65.957867
29.997	940[d]	**$C^{18}O$**	29.999160	67.964	6,272	*HCl_2*	67.966678
30.046	≤100[d]	**C_2H_6**	30.046950	78.053	7[d]	**C_6H_6**	78.046950
31.972	≤8[d]	**^{32}S**	31.972071	80.947	1	*NSCl*	80.943998

[a]Observed and calculated counts. [b]Italics: tentative assignment. [c]Parent and/or fragment ion. [d]Calculated counts.

first fragmentation product ($[M\text{-}H]^+$) were not possible. Instead, identities were assigned using the following rationale:

1. Assignment of ≤10 counts for S^+ at 51.3 km was predicated upon devolving isobaric $O_2{}^+$, which was the dominant species across the mass pair of 32.972 and 32.990 amu. Per Figure 1i, regressions (LAD) using the described constraints provided 0 counts for S^+, which implied an absence of H_2S^+; however, fits to the data were modest, per the summed absolute deviation (SAD) value of ~59 – where SAD values approaching 0 indicated better fits). Per Figure 1j, fits were better minimized (SAD, ~0.04) and yielded 10 counts when using expanded variances for the calculated mass (averaged Δamu plus the standard deviation) and calcualted FWHM (2x the standard deviation).
2. Counts were assigned to ^+P. Per Figures 1k–1n, fits to the mass pair at 30.973 and 31.006 amu revealed discernable peaks with differing peak ratios for P^+ and HNO^+ across the altitudes of 59.9–51.3 km. Regressions (LAD) to the mass pair across these altitudes were maximally minimized when including two species, P^+ and HNO^+, as indicated by the range in SAD values of 1.6×10^{-6} to 9.8×10^{-5}. In comparison, fits using only HNO^+ provided SAD values of ~2.1–5.7. Calculated counts for P^+ were the highest at 51.3 km, and below the detection limit at ≥61.9 km. This suggested the presence of a heterogeneously mixed, phosphorus-bearing, and neutrally charged parent gas or vapor in the middle clouds.
3. Across 64.1–50.3 km, the counts at 34 amu represented H_2S^+ (**33.987721 amu**), $^+PH_3$ (**33.997382 amu**), or a composite of H_2S^+ and $^+PH_3$. Reasonable fits were obtained across the mass triplet at 34 amu (33.966, 33.992, and 34.005 amu) when using single species (Figures 1o and 1p). For H_2S^+ or $^+PH_3$ (at 51.3 km), SAD values from the regressions (LAD) were both ~4.7. Surprisingly, inclusion of a composite provided a better fit with a lower SAD value of ~4.0 (at 51.3 km), per Figure 1q, with regressions (LAD) yielding 18% H_2S (4 counts) and 82% PH_3 (19 counts).
4. The counts of 18 at 32.985 amu represented HS^+ (**32.979896 amu**), $^+PH_2$ (**32.989557 amu**), or a composite of HS^+ and $^+PH_2$.
5. The fragment ^+PH (**31.981732 amu**) was not available for detection due to being masked by $^+O_2$ (31.990 amu, **31.99000 amu**; counts = 356), which was ~30-fold higher in abundance than the $^+PH_3$ parent ion

(calculated counts = 10), and >200-fold higher than the expected counts of ~1.5 for $^{+}$PH, per the NIST reference.

6. When considering deuterium and other isotopologues (51.3 km), the counts of 12 at 35.005 amu were attributed to HDS^{+} (**33.987721 amu**), $^{+}PH_2D$ (**33.997382 amu**), and/or $H_2{}^{33}S$ (**34.987109 amu**).
7. In the data, when considering the conditions of the middle clouds (~74°C, ~ 1 bar, ~50 km), no other parent neutral gases, other than PH_3, could fully account for the presence of $^{+}$P. Alternative gaseous/vaporous and mineralized chemicals included PCl_3, H_3PO_4, and P_2O_5; however, these species could not be fully accounted for in the data or were considered incompatible with the LNMS inlets.
   a) For PCl_3, (1) the parent ion of $^{+}PCl_3$ was isobaric with $^{136}Xe^{+}$ (a high abundance calibrant) and could not be confirmed, (2) the mass for $^{+}PCl_2$ (**100.911612 amu**) likely corresponded to 0 counts (or counts of <0.5) at 100.990 amu (51.3 km), and (3) the mass for $^{+}$PCl (**65.942760 amu**) was not sampled by the LNMS.
   b) For H_3PO_4, many of the potential fragment ions were isobaric with $SO_x{}^{+}$ species and/or possessed counts of 0 (at 51.3 km): (1) at 47.966 amu, the counts of 10 were attributed to SO^{+} (**47.967071 amu**) and/or HPO^{+} (**47.976732 amu**), (2) at 63.962 amu, counts of 5 were attributed to $SO_2{}^{+}$ (**63.962071 amu**) and/or $HPO_2{}^{+}$ (**63.971732 amu**), (3) at 79.958 amu, counts of 0 (or <0.5) were attributed to $SO_3{}^{+}$ (**79.957071 amu**) and/or $HPO_3{}^{+}$ (**79.966732 amu**), and (4) counts of 0 were recorded at masses (81.975 and 96.667 amu) potentially attributed to $H_3PO_3{}^{+}$ and $H_2PO_4{}^{+}$ (**81.982382** and **96.969557 amu**).
   c) For H_2SO_4, which is structurally similar to H_3PO_4, fragmentation to S^{+} occurs in insignificant yields (≤1% of the parent ion; <0.5% of the base peak, $SO_3{}^{+}$) per the NIST reference. For the LNMS, initial calculations suggest a ~6% yield for S^{+} from H_2SO_4 during the clog (36.8 km), where the LNMS was enriched in sulfuric acid fragments. By extension, yields for fragmentation of H_3PO_4 to P^{+} may also be very low.
   d) For P_2O_5, the mass profile likely overlapped with 142.486 amu (2 counts), however, survival of the parent ion through the pinched and low-conductance gas inlets was considered to be unlikely (similar to H_2SO_4; Section 2.4).

In summary, for PH_3, measured counts at 51.3 km potentially correlated to $^{+}$P, $^{+}PH_2$, $^{+}PH_3$, and $^{+}PH_2D$; while counts for $^{+}$PH were masked by O_2. In this analysis, no other viable parent ions could account for $^{+}$P— though this did not exclude $^{+}$P arising from a dissociated $H_xP_yO_z$ species. For H_2S, measured masses correlated to S^{+}, HS^{+}, H_2S^{+}, and HDS^{+}, with regressions indicating 0–10 counts for S^{+}, and minimal abundances of $^{34}S^{+}$. Regressions to the mass triplet at 34 amu (Figures 1q–1s) were supportive of the following composites listed in order of increasing altitude:

- At 50.3 km (SAD, ~1.1), where the clog began to occur during descent: ~50% H_2S^{+} and ~50% $PH_3{}^{+}$ (~4 counts each)
- At 51.3 km (SAD, ~4.0): ~18% H_2S^{+} (~4 counts) and ~82% $^{+}PH_3$ (~19 counts)
- At 55.4 km, through relatively moderate fits (SAD, ~4.8): ~28% H_2S^{+} (~2 counts) and 72% $^{+}PH_3$ (~5 counts)
- Between 58.3-61.9 km (SAD <3.7): A decrease from ~4 to ~2 for H_2S^{+}, and a range of ~0–0.1 for $^{+}PH_3$
- At 64.2 km: Both ions were below or at the detection limit

Comparison to the NIST spectral references revealed similar fragmentation patterns for $^{+}PH_3$ and H_2S^{+} (Figures 1t–1u), respectively. The higher relative yields for HS^{+} and $^{+}PH_2$ were supportive of counts arising from fragmentation of HDS^{+} and $^{+}PH_2D$. Relative abundances for $^{+}$P were similar to the NIST reference, while expected abundances of S^{+} (~2 counts, 51.3 km) fell within the calculated range of 0–10 counts. These complementary abundances were obtained from fits to 31, 32, 34, and 35 amu, which lent support to the peak-fitting model.

For the deuterium isotopologues, across 59.9–50.3 km, substantially high D/H ratios with large propagated errors (~50%–400%) were obtained due to the low counts. For these calculations, counts for PH_2D and HDS at each altitude were corrected for $^{35}Cl^{+}$ (using fits across the mass pair at 35 amu), corrected for $H_2{}^{33}S^{+}$ (using the $^{33}S/^{32}S$ ratio obtained from $^{33}SO^{+}$ and $^{32}SO^{+}$; Section 3.4), and disambiguated using the calculated $PH_3{}^{+}/H_2S^{+}$ ratio given the similar degrees of hydrogen-deuterium exchange for PH_3 and H_2S (Fernández-Sánchez & Murphy, 1992; Jones & Sherman, 1937; Wada & Kiser, 1964; Weston Jr. & Bigeleisen, 1952).

At 51.3 km, this provided high D/H ratios of $1.0 \times 10^{-2} \pm 0.5 \times 10^{-2}$ for PH_3 and $1.6 \times 10^{-2} \pm 1.0 \times 10^{-2}$ for H_2S, which were suggestive of underestimations of the $H_2{}^{33}S$ abundances and/or large variance in the lower counts. In support, the composite isotopologue ratio ($(PH_2D + HDS)/(PH_3+H_2S)$) at 51.3 km was 0.63 and decreased >1,000-fold to 0.045 ± 0.021 between ~24 and 0.9 km, where counts were substantially larger, and representative of less statistical variation. This composite isotopologue ratio was calculated using uncorrected counts at 35.005 amu (PH_2D + HDS) and 33.992 (PH_3+H_2S). We note that Donahue and Hodges (1993) reported a similar ratio of 0.05 for HDS/H_2S using the same mass points and uncorrected counts below the clouds.

2.3. Brønsted-Lowry Acids

The LNMS data contained counts for masses consistent with HNO_3^+, HNO_2^+, NO_2^+, HNO^+, NO^+, ^+OH, O^+, and N^+ (Table S1). Devolved plots at 31 amu (Section 3.2) supported the presence of HNO^+. Fragmentation products of HNO_3, per published reports (Friedel et al., 1959; O'Connor et al., 1997), do not include HNO^+ or HNO_2^+. For HNO_2, we found conflicting evidence for HNO^+ as a fragmentation product; with spectra from PubChem (CID 386662) supporting HNO^+ (Figure S4). Together, this was suggestive of HNO_3^+ and HNO_2^+ being parent ions, and nitroxyl hydride (HNO^+) being a fragment of HNO_2^+. Counts for NO^+ (~413) and NO_2^+ (≤620), the base peaks of HNO_2^+ and HNO_3^+, were estimated by disambiguating the isobaric species of $C^{18}O^+$ and $CO^{18}O^+$, respectively (Supporting Information). Per Figure S4, fragmentation patterns for HNO_2^+ followed the general trend of the reference. Potential isobaric and co-present species included PO^+ (**46.968910 amu**) and PO_2^+ (**62.963907 amu**).

The mass data also revealed assignments for HCl and HCN (Table S1), and possibly HF and $HClO_2$. Across the mass pair of 35.966 and 35.981 amu, $H^{35}Cl$ was a potential minor component against the major isobar of $^{36}Ar^+$. Similarly, at 37.968 amu, $H^{37}Cl$ was a minor component against the major isobar of $^{38}Ar^+$. At 51.3 km, fits to 35 amu (34.972 & 35.005 amu) provided calculated counts of 12 for $^{35}Cl^+$. When assuming HCl to be the parent source, per yields from the NIST reference, this amounted to ~80 counts for $H^{35}Cl^+$. For $^{37}Cl^+$, counts were corrected for $C_3H_1^+$, a benzene fragment, (see Supporting Information), and for $D^{35}Cl^+$ using a $(D/H)_{HCl}$ ratio of 0.0303 from 74 km (Krasnopolsky et al., 2013). Across the altitudes of 58.3–51.3 km, this yielded a $^{37}Cl/^{35}Cl$ ratio of $4.5 \times 10^{-1} \pm 0.7 \times 10^{-1}$ comparable to the terrestrial value (Table S2).

At the respective positions of 26 and 27 amu, HCN^+ (**27.010899 amu**) and CN^+ (**26.003074 amu**) were likely the dominant species, with HCN being the dominant parent source. At best, the isobaric species of $C_2H_3^+$ and $C_2H_2^+$ (Section 3.6) were minor constituents in the peak profiles for HCN^+ and CN^+, respectively. Similarly, HF^+ was likely a minor component against the isobaric species $H_2{}^{18}O^+$ and $^{20}Ne^+$; as was F^+ against the isobaric species of $^{18}OH^+$ and $^{40}Ar^{++}$. For $HClO_2$, the counts at 50.969 amu was consistent with assignment of ClO^+ (**50.963853 amu**), while counts at 66.963 and 67.964 amu were tentatively assigned to composites of ClO_2^+ (**66.958853 amu**) with $^{134}Xe^{++}$ (**66.952697 amu**), and $HClO_2^+$ (**67.966678 amu**) with $^{136}Xe^{++}$ (**67.953610 amu**), respectively.

2.4. Oxysulfur Species

The data supported the presence of several potential fragments of H_2SO_4 (with counts ranging from 2 to 10), including $^{33}SO^+$, $^{34}SO^+$, $^{33}SO_2^+$, $^{34}SO_2^+$, and potentially HSO_2^+ (Table S1). Fragmentation yields (Figure S4), however, were dramatically different from the NIST reference (no counts were observed for $H_2SO_4^+$) due to the impact of viscous flow through the crimped inlets of the LNMS, which promoted dissociation of H_2SO_4 at the inlet before entering the ion source (Hoffman, Hodges, Donahue, et al.., 1980). Given the presence of water in the data (especially during the clog), the H_2SO_4 was presumably acquired from aerosolized species and not vapor. Per Section 3.1 (Step 6b), SO_3^+, SO_2^+, and SO^+ were respectively isobaric to HPO_3^+, HPO_2^+, and HPO^+. However, counts from SO^+ were suggestive of $^{33}S/^{32}S$ and $^{34}S/^{32}S$ ratios of $1.3 \times 10^{-2} \pm 0.9 \times 10^{-2}$ and $5.9 \times 10^{-2} \pm 0.8 \times 10^{-2}$ across the altitudes of 39.3 and 24.4 km, respectively, where the LNMS was enriched in sulfuric acid fragments. For SO_2^+, this amounted to disentangled counts of 0.3 for $^{34}SO_2^+$, which indicated that $^{132}Xe^{++}$ (**65.952077 amu**) was the major species at 65.961 amu. Similarly, the isobars of $^{130}Xe^{++}$, $^{33}SO_2^+$, and HSO_2^+ were likely mixed at 64.960 amu. The LNMS data suggested the presence of several Xe isotopes, including ^{128}Xe, ^{129}Xe, ^{130}Xe, ^{132}Xe, and ^{134}Xe.

2.5. Ammonia

Table S1 lists the mass data and assignments potentially consistent with $^{+}NH_2D$, $^{+}NH_3$ (ammonia), $^{+}NH_2$, ^{+}NH, ^{+}N, and the isobars of water and methane-related species. For water (Figures 1c and S1), fits to the mass triplet at 18 amu (17.985, 18.010, and 18.034 amu) were best minimized when including ~47 counts from $^{+}NH_2D$ (**18.032826 amu**); SAD values from fits to H_2O and H_2O/NH_2D were ~25 and 0.8, respectively (inclusion of $^{+}NH_2D$ yielded no changes to the FWHM for water or averaged Δamu at 51.3 km). The assignment of $^{+}NH_2D$, while tentative, was supportive of NH_3^+ being the parent species. In the data, the mass at 17.026 amu was consistent with $^{+}NH_3$ (**17.026549 amu**); however, $^{13}CH_4^+$ (**17.034655 amu**) was the dominant species at this position (due to use of CH_4 as a calibrant). Likewise, masses potentially consistent with $^{+}NH_2$ (16.019 amu) and ^{+}NH (15.013 amu) were dominated by the isobars of $^{12}CH_4^+$ (**16.031300 amu**) and $^{12}CH_3^+$ (**15.023475 amu**), respectively.

2.6. Low-Mass Organics

Table S1 lists the mass data and assignments for methane (CH_4), ethane (C_2H_6), benzene (C_6H_6), and related fragments. Across all altitudes (64.2–0.9 km), fragmentation of CH_4 yielded CH_3^+ in relative abundances of 76 ± 6%, similar to the NIST and MassBank references (~83%–89%). Atomic carbon in the LNMS data was enriched as expected due to tremendous input from CO_2.

For ethane (C_2H_6), the LNMS data possessed pre-selected masses consistent with $C_2H_6^+$, $C_2H_5^+$, $C_2H_4^+$, $C_2H_3^+$, and $C_2H_2^+$. Per our model, these species were likely minor components against the isobaric alternatives of $C^{18}O^+$, $^{13}CO^+$, N_2^+ and CO^+, CN^+, and HCN^+, respectively. Fits to 30, 27, and 26 amu were indicative of $C_2H_6^+$ (≤100 counts), $C_2H_3^+$ (≤50 counts), and $C_2H_2^+$ (≤10 counts) being constituents of the peaks dominated by $^{12}C^{18}O^+$, HCN^+, and CN^+, respectively.

For benzene, the data (at 51.3 km) possessed counts corresponding to $C_5{}^{13}CH_6^+$ ($(M+1)^+$), $C_6H_6^+$ (M^+), and $C_6H_5^+$ ($[M-H]^+$) at 78.924, 78.053, and 77.040 amu, respectively. As described in the Supporting Information, disambiguation of the counts (based on the abundances of $C_6H_5^+$ and $C_5{}^{13}CH_6^+$) suggested the presence of isobaric species at 78.053 amu such as dimethyl sulfoxide ($(CH_3)_2SO^+$) and/or P_2O^+. Finally, in this model, C_3H_4 (propyne) was indistinguishable against the mass peak for $^{40}Ar^+$ (Figure 1e).

3. Discussion

Assignments to the LNMS data reveal fragmentation products and parent ions that support the presence of novel chemical species in Venus' atmosphere. Atomic phosphorus was among the assignments; thereby, indicating the presence of a phosphorus-bearing gas or vapor in Venus' clouds. Across the altitudes of 58.3–51.3 km, phosphine (PH_3) represented the simplest phosphorus-bearing gas that fit the LNMS data best. While H_3PO_4 remains a viable candidate, matches to the combined data require very high vaporous or aqueous aerosol abundances relative to H_2SO_4. Additionally, while counts in the data support the presence of P_2O_5, a proposed suspended mineral in Venus' clouds (Krasnopolsky, 1989), it is our understanding that the LNMS inlets were designed to restrict the entry of such types of molecules. We were also unable to find literature precedent for $P_2O_5^+$ as a parent ion under conditions similar to the LNMS or NIST references. Alternative gaseous candidates included (1) phosphorus trichloride (PCl_3), which was inadequately described by the data, (2) elemental phosphorus (P_4), phosphorus dioxide (PO_2), and phosphorus monoxide (PO), which are not gases under the conditions of Venus' clouds, and (3) diphosphorus oxide (P_2O), which is an unstable gas that potentially serves as dissociative (e.g., at the inlet) and/or fragmentation product from a larger P_xO_y species; however, we were unable to find literature precedent for P_2O^+ as a mass spectral fragmentation product or parent ion. Thus, we propose that phosphine and H_2S are potentially co-present in the middle clouds.

The LNMS data additionally support the presence of acidic species, including HNO_2, HNO_3, HCl, HCN, and possibly HF and $HClO_2$. The presence of HNO_2^+ is supported by assignments of the fragment products of HNO^+ and NO^+, and preliminary analyses show that HNO_2^+ and HNO^+ track well across the altitude profile toward the surface. Assignments of NO_2^+ and NO^+ support HNO_3^+, where counts for HNO_3^+ substantially increase from 1 (at 51.3 km) to ~720 below the clouds. When considering all potential nitrogen parent

species, the LNMS data support a range in nitrogen oxidation numbers (or states), including −3 (HCN and possibly NH_3), 0 (N_2), +3 (HNO_2), and +5 (HNO_3).

The LNMS data additionally show the presence of CO, O_2, and possibly COS and NSCl; however, fragmentation products for COS and NSCl, other than the atomic ions, could not be identified. Comparison of the CO_2 fragmentation patterns revealed a $CO^+/CO_2{}^+$ ratio of ∼0.16–0.24 at 51.3 km in the LMNS data compared to ∼0.10 from the NIST reference. Per Hoffman et al. (1979b), a $CO^+/CO_2{}^+$ ratio of ∼0.4 was obtained when the gate valve to the ion source in the LMNS was closed. At an altitude of 51.3 km (∼1 bar), however, we presume that the gate valve was open. Thus, the $CO^+/CO_2{}^+$ ratio was supportive of CO^+ being an atmospheric parent species, where corresponding abundances were disambiguated using the $CO^+/CO_2{}^+$ ratios from the NIST and LNMS spectra. The data also support the presence of oxygen gas (O_2), which Hoffman, Hodges, Donahue, et al. (1980) attributed to dissociative ionization of CO_2. While the NIST spectrum for CO_2 (Figure S3) shows no formation of O_2, the possibility of a ∼0.02% yield from $\sim 1.8 \times 10^6$ counts of CO_2 to give ∼320 counts of $O_2{}^+$ could not be excluded. Finally, using isotopologues of CO_2, N_2, and SO, and atomic Cl (at select altitudes, Table S2), we obtained isotope ratios for $^{13}C/^{12}C$ ($1.33 \times 10^{-2} \pm 0.01 \times 10^{-2}$), $^{15}N/^{14}N$ ($2.63 \times 10^{-3} \pm 0.86 \times 10^{-3}$), $^{18}O/^{16}O$ ($2.18 \times 10^{-3} \pm 0.17 \times 10^{-3}$), $^{33}S/^{32}S$ ($1.4 \times 10^{-2} \pm 0.9 \times 10^{-2}$), $^{34}S/^{32}S$ ($5.8 \times 10^{-2} \pm 0.7 \times 10^{-2}$), and $^{37}Cl/^{35}Cl$ ($4.5 \times 10^{-1} \pm 0.7 \times 10^{-1}$) – which were similar to terrestrial values (Table S2) (Farquhar, 2017; Haynes, 2016).

4. Conclusion

Our assessment of the PV LNMS data supports a composition in the middle clouds that includes the main group hydrides of hydrogen sulfide, phosphine, water, ethane, and possibly ammonia; along with several redox-active acids including nitrous acid, nitric acid, sulfuric acid, hydrogen cyanide, and potentially chlorous acid, along with the monoprotic acids of hydrochloric acid and potentially hydrogen fluoride. In total, these assignments illuminate a potential for acid-mediated redox disequilibria within the clouds.

Disequilibria in the lower atmosphere of Venus was discussed by Florenskii et al. (1978), in regards to Venera 8 observations of NH_3 (Surkov et al., 1973), and by Zolotov (1991). These LNMS and Venera 8 observations suggest that disparate chemicals across varying equilibrium states may be sustained by unknown chemistries. We speculate that this includes the injection of appreciable reducing power through volcanism or surface outgassing (e.g., Gülcher et al., 2020 Ivanov and Head, 2013; Shalygin et al., 2015).

Regarding the hypothetical habitability of Venus' clouds, our assignments reveal a potential signature of anaerobic phosphorus metabolism (phosphine), a potential electron donor for anoxygenic photosynthesis (nitrous acid; nitrite) (Griffin et al., 2007), and all major constituents of the terrestrial nitrogen cycle (nitrate, nitrite, possibly ammonia, and N_2) (Madigan et al., 2014). Also, the redox pair of nitrate and nitrite support the postulate by Limaye et al. (2018) of a hypothetical iron-sulfur cycle in Venus' clouds.

Looking ahead, high-resolution (RP > 5,000) untargeted and targeted mass spectral approaches through sustained aerial platforms and descending probes would significantly aid in elucidating the gaseous and aerosol compositions in the clouds and atmosphere. The DAVINCI+ mission design concept currently under consideration by NASA serves as an excellent step toward this goal.

Conflict of Interests

All authors declare that there are no conflict of interests.

Data Availability Statement

All LNMS data used in this study were obtained from published reports (Hoffman, Hodges, Donahue, et al., 1980; Hoffman, Hodges, Wright, et al., 1980). The LNMS archive data across all altitudes were posted online on October 8, 2020 by the NASA Space Science Data Coordinated Archive (NSSDC) (https://nssdc.gsfc.nasa.gov/nmc/dataset/display.action?id=PSPA-00649).

Acknowledgments
It is a pleasure to acknowledge R. Richard Hodges for insightful discussions regarding the LNMS operation, data, and history. Rakesh Mogul acknowledges support from the National Aeronautics and Space Administration (NASA) Research Opportunities in Space and Earth Sciences (Grant no. NNH18ZDA001N). Sanjay S. Limaye was supported by NASA (Grant no. NNX16AC79G). M. J. Way was supported by the NASA Astrobiology Program through collaborations arising from his participation in the Nexus for Exoplanet System Science (NExSS) and the NASA Habitable Worlds Program. M. J. Way also acknowledges support from the GSFC Sellers Exoplanet Environments Collaboration (SEEC), which is funded by the NASA Planetary Science Division's Internal Scientist Funding Model. JAC acknowledges the support of the Genome Sciences Training Program at University of Wisconsin, Madison.

References

Bains, W., Petkowski, J. J., Seager, S., Ranjan, S., Sousa-Silva, C., Rimmer, P. B., et al. (2020). *Phosphine on Venus cannot be explained by conventional processes*. arXiv:2009.06499. https://arxiv.org/abs/2009.06499

Donahue, T. M., & Hodges, R. R. (1992). Past and present water budget of Venus. *Journal of Geophysical Research*, *97*, 6083–6091. https://doi.org/10.1029/92je00343

Donahue, T. M., & Hodges, R. R. (1993). Venus methane and water. *Geophysical Research Letters*, *20*(7), 591–594. https://doi.org/10.1029/93gl00513

Donahue, T. M., Hoffman, J. H., Hodges, R. R., & Watson, A. J. (1982). Venus was wet: A measurement of the ratio of deuterium to hydrogen. *Science*, *216*, 630–633. https://doi.org/10.1126/science.216.4546.630

Encrenaz, T., Greathouse, T. K., Marcq, E., Widemann, T., Bézard, B., Fouchet, T., et al. (2020). A stringent upper limit of the PH3 abundance at the cloud top of Venus. *Astronomy & Astrophysics*, *643*, L5. https://doi.org/10.1051/0004-6361/202039559

Farquhar, J. (2017). Sulfur isotopes. In W. M. White, (Ed.), *Encyclopedia of geochemistry: A comprehensive reference source on the chemistry of the Earth* (pp. 1–8). Springer International Publishing.

Fernández-Sánchez, J. M., & Murphy, W. F. (1992). Raman scattering cross sections and polarizability derivatives of H_2S, D_2S, and HDS. *Journal of Molecular Spectroscopy*, *156*(2), 431–443. https://doi.org/10.1016/0022-2852(92)90244-i

Florenskii, C. P., Volkov, V. P., & Nikolaeva, O. V. (1978). A geochemical model of the Venus troposphere. *Icarus*, *33*, 537.

Friedel, R. A., Shultz, J. L., & Sharkey, A. G. (1959). Mass spectrum of nitric acid, *Analytical Chemistry*, *31*(6), 1128. https://doi.org/10.1021/ac60150a615

Greaves, J. S., Bains, W., Petkowski, J. J., Seager, S., Sousa-Silva, C., Ranjan, S. et al. (2020). *On the robustness of phosphine signatures in Venus' clouds*. arXiv:2012.05844.

Greaves, J. S., Richards, A. M. S., Bains, W., Rimmer, P. B., Clements, D. L., S. Seager, et al. (2020). *Re-analysis of phosphine in Venus' clouds*. arXiv:2011.08176. https://arxiv.org/abs/2011.08176

Greaves, J. S., Richards, A. M. S., Bains, W., Rimmer, P. B., Sagawa, H., Clements, D. L., et al. (2020). Phosphine gas in the cloud decks of Venus. *Nature Astronomy*, 1–10.

Griffin, B. M., Schott, J., & Schink, B. (2007). Nitrite, an electron donor for anoxygenic photosynthesis. *Science*, *316*(5833), 1870. https://doi.org/10.1126/science.1139478

Gülcher, A. J. P., Gerya, T. V., Montési, L. G. J., & Munch, J. (2020). Corona structures driven by plume–lithosphere interactions and evidence for ongoing plume activity on Venus. *Nature Geoscience*, *13*, 547–554.

Haynes, W. M. (2016). *CRC handbook of chemistry and physics*. Boca Raton, FL: CRC Press.

Hoffman, J. H., Hodges, R. R., Donahue, T. M., & McElroy, M. B. (1980). Composition of the Venus lower atmosphere from the Pioneer Venus mass spectrometer. *Journal of Geophysical Research*, *85*(A13), 7882–7890. https://doi.org/10.1029/ja085ia13p07882

Hoffman, J. H., Hodges, R. R., & Duerksen, K. D. (1979). Pioneer Venus large probe neutral mass spectrometer. *Journal of Vacuum Science and Technology*, *16*(2), 692–694. https://doi.org/10.1116/1.570059

Hoffman, J. H., Hodges, R. R., McElroy, M. B., Donahue, T. M., & Kolpin, M. (1979a). Venus lower atmospheric composition: Preliminary results from Pioneer Venus. *Science*, *203*(4382), 800–802. https://doi.org/10.1126/science.203.4382.800

Hoffman, J. H., Hodges, R. R., McElroy, M. B., Donahue, T. M., & Kolpin, M. (1979b). Composition and structure of the Venus atmosphere: Results from Pioneer Venus. *Science*, *205*(4401), 49–52. https://doi.org/10.1126/science.205.4401.49

Hoffman, J. H., Hodges, R. R., Wright, W. W., Blevins, V. A., Duerksen, K. D., & Brooks, L. D. (1980). Pioneer Venus sounder probe neutral gas mass spectrometer. *IEEE Transactions on Geoscience and Remote Sensing*, *GE-18*(1), 80–84. https://doi.org/10.1109/tgrs.1980.350286

Hoffman, J. H., Oyama, V. I., & Von Zahn, U. (1980). Measurements of the Venus lower atmosphere composition: A comparison of results. *Journal of Geophysical Research*, *85*(A13), 7871–7881. https://doi.org/10.1029/ja085ia13p07871

Ivanov, M. A., & Head, J. W. (2013). The history of volcanism on Venus. *Planetary and Space Science*, *84*, 66–92. https://doi.org/10.1016/j.pss.2013.04.018

Johnson, N. M., & Oliveira, M. R. R. (2019). Venus atmospheric composition in situ data: A compilation. *Earth and Space Science*, *6*(7), 1299–1318. https://doi.org/10.1029/2018ea000536

Jones, T., & Sherman, A. (1937). Calculation of equilibrium constants and activation energies for some reactions involving various isotopic species of hydrogen, water, and hydrogen sulfide. *The Journal of Chemical Physics*, *5*(6), 375–381. https://doi.org/10.1063/1.1750044

Kliore, A. J., Moroz, V. I., & Keating, G. (1985). The Venus international reference atmosphere. *Advances in Space Research*, *5*(11), 8–305. https://doi.org/10.1016/0273-1177(85)90196-6

Krasnopolsky, V. A. (1989). Vega mission results and chemical composition of Venusian clouds. *Icarus*, *80*(1), 202–210. https://doi.org/10.1016/0019-1035(89)90168-1

Krasnopolsky, V. A., Belyaev, D. A., Gordon, I. E., Li, G., & Rothman, L. S. (2013). Observations of D/H ratios in H_2O, HCl, and HF on Venus and new DCl and DF line strengths. *Icarus*, *224*(1), 57–65. https://doi.org/10.1016/j.icarus.2013.02.010

Kumar, S., Hunten, D. M., & Taylor, H. A., Jr. (1981). H_2 abundance in the atmosphere of Venus. *Geophysical Research Letters*, *8*(3), 237–240. https://doi.org/10.1029/gl008i003p00237

Limaye, S. S., Mogul, R., Smith, D. J., Ansari, A. H., Słowik, G. P., & Vaishampayan, P. (2018). Venus' spectral signatures and the potential for life in the clouds. *Astrobiology*, *18*(9), 1181–1198. https://doi.org/10.1089/ast.2017.1783

Madigan, M. T., Martinko, J. M., Bender, K. S., Buckley, D. H., & Stahl, D. A. (2014). *Brock biology of microorganisms*. Pearson.

Moroz, V. (1981). The atmosphere of Venus. *Space Science Reviews*, *29*(1), 3–127. https://doi.org/10.1007/bf00177144

O'Connor, C. S., Jones, N. C., & Price, S. D. (1997). Electron-impact ionization of nitric acid. *International Journal of Mass Spectrometry and Ion Processes*, *163*(1–2), 131–139. https://doi.org/10.1016/s0168-1176(96)04536-3

Oyama, V. I., Carle, G. C., Woeller, F., Pollack, J. B., Reynolds, R. T., & Craig, R. A. (1980). Pioneer Venus gas chromatography of the lower atmosphere of Venus. *Journal of Geophysical Research*, *85*, 7891–7902. https://doi.org/10.1029/ja085ia13p07891

Pollack, J. B., Dalton, J. B., Grinspoon, D., Wattson, R. B., Freedman, R., Crisp, D., et al. (1993). Near-infrared light from Venus' nightside: A spectroscopic analysis. *Icarus*, *103*(1), 1–42. https://doi.org/10.1006/icar.1993.1055

Roth, E., Holden, N., Barnes, I., de Bievre, P., Johnson, W., Martin, R., et al. (1976). Atomic weights of the elements 1975. *Pure and Applied Chemistry*, *47*(1), 75–95.

Seager, S., Petkowski, J. J., Gao, P., Bains, W., Bryan, N. C., Ranjan, S., & Greaves, J. (2020). The Venusian lower atmosphere haze as a depot for desiccated microbial life: A proposed life cycle for persistence of the Venusian aerial biosphere. *Astrobiology*. https://doi.org/10.1089/ast.2020.2244

Shalygin, E. V., Markiewicz, W. J., Basilevsky, A. T., Titov, D. V., Ignatiev, N. I., & Head, J. W. (2015). Active volcanism on Venus in the Ganiki Chasma rift zone. *Geophysical Research Letters*, *42*(12), 4762–4769. https://doi.org/10.1002/2015gl064088

Smirnova, T., & Kuz'min, A. (1974). Water-vapor and ammonia abundance in the lower atmosphere of Venus estimated from radar measurements. *Soviet Astronomy*, *18*, 357.

Snellen, I., Guzman-Ramirez, L., Hogerheijde, M., Hygate, A., & van der Tak, F. (2020). Re-analysis of the 267 GHz ALMA observations of Venus—No statistically significant detection of phosphine. *Astronomy & Astrophysics*, *644*, L2.

Stark, H., Yatavelli, R. L. N., Thompson, S. L., Kimmel, J. R., Cubison, M. J., Chhabra, P. S., et al. (2015). Methods to extract molecular and bulk chemical information from series of complex mass spectra with limited mass resolution. *International Journal of Mass Spectrometry*, *389*, 26–38. https://doi.org/10.1016/j.ijms.2015.08.011

Surkov, I. A. (1977). *Geochemical studies of Venus by Venera 9 and 10 automatic interplanetary stations.*, Paper presented at Lunar and Planetary Science Conference Proceedings.

Surkov, Y. A., Andrejchikov, B. M., & Kalinkina, O. M. (1973). On the content of ammonia in the Venus atmosphere based on data obtained from Venera 8 automatic station. *Akademiia Nauk SSSR Doklady*, *213*, 296.

Urban, J., Afseth, N. K., & Štys, D. (2014). Fundamental definitions and confusions in mass spectrometry about mass assignment, centroiding and resolution. *TRAC Trends in Analytical Chemistry*, *53*, 126–136. https://doi.org/10.1016/j.trac.2013.07.010

Villanueva, G., Cordiner, M., Irwin, P., de Pater, I., Butler, B., Gurwell, M., et al. (2020). *No phosphine in the atmosphere of Venus*. arXiv:2010.14305. https://arxiv.org/abs/2010.14305

Von Zahn, U., & Moroz, V. I. (1985). Composition of the Venus atmosphere below 100 km altitude. *Advances in Space Research*, *5*(11), 173–195. https://doi.org/10.1016/0273-1177(85)90201-7

Wada, Y., & Kiser, R. W. (1964). Mass spectrometric study of phosphine and diphosphine. *Inorganic Chemistry*, *3*(2), 174–177. https://doi.org/10.1021/ic50012a004

Weston, R. E. Jr, & Bigeleisen, J. (1952). Equilibrium in the exchange of hydrogen between phosphine and water. *The Journal of Chemical Physics*, *20*(9), 1400–1402. https://doi.org/10.1063/1.1700770

Zolotov, M. Y. (1991), *Redox conditions of the near surface atmosphere of Venus. II. Equilibrium and disequilibrium models.* Paper presented at Lunar and Planetary Science Conference, p. 1573.